ACTA STEREOL 1999; 18/3: 305-312
ORIGINAL SCIENTIFIC PAPER

ELEVATED TEMPERATURE EFFECTS ON THE STRUCTURAL PARAMETERS IMPORTANT IN CORROSION OF DUPLEX STAINLESS STEEL

Zorica Cvijović[1] , Vida Knežević[1] , Draginja Mihajlović[1] , Goran Radenković[2]

[1] Faculty of Technology and Metallurgy, University of Belgrade, Karnegijeva 4, 11001 Belgrade, POB. 494, Yugoslavia
[2] Faculty of Mechanical Engineering, University of Niš, Beogradska 14, 18000 Niš, Yugoslavia

ABSTRACT

A quantitative characterization of the microstructural changes in gas (GTA) surface melted duplex stainless steel (DSS) when subjected to annealing at 900°C for times up to 120 minutes was carried out in order to correlate the structural parameters with pitting corrosion resistance. The kinetics of δ ferrite transformation and coarsening of the initial lathy ferrite structure were monitored by estimating the volume fraction of phases, V_V, surface area of the interphase boundary in a unit volume, S_V, and the ratio of these two parameters, S_V/V_V. The corrosion testing was performed in 0.5 M NaCl solution at room temperature using potentiodynamic and potentiostatic polarization techniques. It has been shown that the applied heat treatment dramatically changed the corrosion behaviour of resolidified DSS. Due to the simultaneous formation of γ_2 and σ-phase, the pitting potential value, E_p, decreased from 570 mV (SCE) for as-resolidified material to 150, 125 and 30 mV (SCE) after annealing for 5, 15 and 30 min, respectively. The high density of fine precipitates caused an increase in the amount of δ/secondary phase boundaries providing more sites for pit nucleation. As a result, numerous, small and regular pits were formed at the interphase boundaries. For longer exposure times (60 and 120 min), the δ transformation was almost complete. The slight increase in the E_p value and changed initial form of attack can be attributed to the different partitioning of alloying elements, due to the extensive σ-phase precipitation within ferrite matrix.

Key words: duplex stainless steel, δ ferrite transformation, high temperature annealing, pitting corrosion behavior, stereological analysis, surface melting.

INTRODUCTION

Duplex stainless steels (DSSs) form a very attractive class of engineering materials possessing a remarkable combination of mechanical strength and corrosion resistance in chloride ion containing solutions and many other environments (Walker, 1988; Wagner and Korkhans, 1995). Therefore, they are widely used in the oil, chemical and power industries as well as in the seawater systems. The superior properties of both the wrought and cast DSSs derive from their chemical compositions and an optimal ferrite/austenite (δ/γ) balance which is established by suitable heat treatment in (δ+γ) region (Kotecki, 1989; Sedriks, 1989; Kane, 1993). Thus, in our earlier study on the impact toughness and susceptibility to pitting corrosion of cast DSS with a pitting resistance equivalent (PRE_N = wt.% Cr + 3.3 wt.% Mo + 16 wt.% N) of 32, the microstructural changes produced by annealing in the range from 1100

to 1250 °C are conducive to attaining a marked increase in its notch impact energy and pitting corrosion resistance in 0.5 M NaCl solution at room temperature (Radenković et al., 1994). Rapid solidification processing (RSP) such as high power density (HPD) plasma arc (PA), electron beam (EB) and laser beam (LB) welding or surface melting, has also proved effective in improving resistance to localized corrosion. The metastable δ formation and homogenization of structure through rapid solidification results in several hundred millivolts ennoblement of the pitting potential and enhancement of the open circuit corrosion resistance due to decrease in both anodic and cathodic current densities (Yoshioka et al., 1986; Radenković et al., 1995).

However, a disadvantage of these rapidly solidified DSSs is the possible metastable δ ferrite decomposition into various secondary phases when they are exposed to high temperature service conditions (Shek et al., 1994; Nilsson et al., 1995). Namely, precipitation of the so-called secondary austenite (γ_2), nitrides, σ- and χ-phases can cause the time-dependent degradation of the material, particularly its corrosion properties. Redristibution of alloying elements as a result of their precipitation may lead to local reductions in pitting resistance and associated corrosion attack, either in regions that are depleted with respect to crucial alloying elements or in the precipitates themselves (Sedriks, 1989; Ogawa and Koseki, 1989; Nilsson et al., 1996). Since the extent of corrosion depends on the type and amount of precipitated phases, as well as the size and shape of δ/secondary phase interfaces as the preferential nucleation sites of pits, it is necessary to quantify the relevant microstructural parameters. Although the large number of articles has been published on the δ transformation, very little information is presently available on the effects of microstructural parameters on susceptibility to localized corrosion of heat-treated DSSs solidified at high cooling rates.

Therefore, this investigation is undertaken to precisely descript the microstructural changes during high-temperature annealing of surface melted CrNiMoCu grade of cast DSS, in order to correlate these changes with the observed variations in the pitting corrosion behaviour.

MATERIALS AND METHODS

To maintain continuity with previous studies (Radenković et al., 1994; Radenković et al., 1995), the base material used in this investigation was a commercial DSS sand cast block, containing (in mass.%) 22.5Cr-7.8Ni-2.3Mo-3.5Cu-0.1N-0.08C. A highly metastable ferritic-austenitic microstructure which may be responsible for a large increase in resistance to pitting corrosion was evaluated by surface melting treatment. The local surface melting was performed on 15x15x10 mm samples by a gas tungsten arc (GTA) welding techniques at power level of 1440 W for duration time of 20 s. After stationary remelting the samples were air cooled to room temperature and subsequently annealed at 900°C, where the chosen DSS was expected to show more rapid precipitation of the γ_2 and σ-phases. Annealing was performed from 2 up to 120 minutes. After the heat treatment, the samples were quenched in cold water.

The microstructural characteristics of the material both in the as-resolidified condition and after high temperature annealing, were established by light optical (LOM) and scanning electron microscopy (SEM). Metallographic sections were electrochemically etched using a solution containing: a) 20 g NaOH + 100 ml H_2O, at U = 1-5 V, for t = 2-20 s, and b) 10 g oxallic acid + 100 ml H_2O, at U = 2-6 V, for t = 10-20 s.

The kinetics of δ transformation and morphological changes have been studied by monitoring the volume fraction of phases, V_V, surface area of the interface boundary in a unit volume, S_V, and the ratio of these two parameters, S_V/V_V. Measurements were carried out on a

section taken parallel and near to the melt surface of remelted zone using a standard image analyzer.

The corrosion testing was performed in 0.5 M NaCl solution at room temperature using cylindrical specimens of 5 mm diameter prepared from central region of remelted zone. Before starting the polarization scan, the metal surface was ground with SiC paper up to N° 2400, successively polished with 1 and 0.3 μm alumine water suspension, rinsed with water and then washed ultrasonically in ethanol. Specimens were immersed into the testing cell in such a way that only their polished surface capillary touched the solution. The characteristic pitting conditions were established by potentiodynamic polarization techniques. Anodic polarization curves were recorded with potential sweep rate of 0.2 mV/s up to the potential above which stable pits were formed. The potential of working electrode was measured against a saturated calomel electrode (SCE). In order to determinate the position of the pitting potential (Ep) more accurately the potentiostatic polarization tests were also performed. When the pits were initiated, the exposure of the specimens were interrupted at regular intervals and the patterns observed on corroded surfaces were examined in detail by LOM and SEM.

RESULTS AND DISCUSSION

A. Initial microstructure

Prior to describing the microstructural changes that occur in GTA surface melted DSS upon annealing, it is of significant interest, for structural stability define purpose, to relate the microstructure evaluated during RSP to that of the conventionally solidified material employed in the previous article (Radenković et al., 1994). Namely, the as-resolidified structure has not attained thermodynamic equilibrium because of the higher cooling rate. Since there is no precise data in the literature on the corresponding equilibrium phase composition of the investigated steel, an approximate evaluation of the deviation from equilibrium can only be performed on the basis of the data for the cast structure, which according to the cooling conditions should be closer to equilibrium state.

The as-cast microstructures of a cast block used for preparing samples for surface melting and resolidified material are illustrated in Fig.1. It reveals a duplex austenite (white) plus ferrite (relatively dark) microstructure in both conditions.

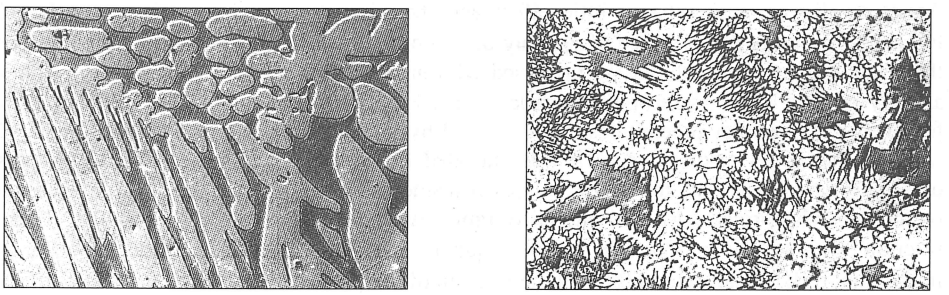

Fig.1. LO micrographs showing effect of cooling rate on the microstructure of DSS. (a) As-cast base material, (b) as-resolidified GTA melt.

An increase of the cooling rate does not change the primary ferrite with second phase austenite (FA) solidification mode (Elmer et al., 1989), however, variation of the cooling rate, achieved by a proper choice of the melting parameters considerably influenced the structure

morphology. The solidification substructure changed from dendritic to predominantly cellular mode and the volume fraction of retained ferrite was greater for about 10 vol.%. Untransformed ferrite stays in the form of platelets with straight and often parallel boundaries of regular width. Consequently, the transition from interdendritic austenite (IDA) to lathy ferrite (LF) microstructure took place. The solid state transformation of ferrite, however, is rather restricted on the vicinity of primary ferrite-eutectic austenite boundary leaving the untransformed blocky ferrite regions with angular edges, Fig.1b. According to Kokawa et al. (1989), the lathy ferrite takes approximately the Kurdjumov-Sachs (K-S) orientation relationship with austenite and this leads to a low-energy δ/γ boundary and higher boundary coherency.

In addition to these variations in microstructure, the surface melting resulted in the increase of microstructural constituents' fineness. Due to reduction in the amount of eutectic, γ_E, and austenite which is formed by the $\delta \rightarrow \gamma$ transformation, γ_T, and formation of thin adjacent γ_T platelets inside the fine ferrite cells, the δ/γ interface amount $S_{V\delta-\gamma}$ and the specific surface $S_{V\delta-\gamma}/V_{V\gamma}$ are increased by a factor of 5 - 5.6 times. Therefore, it may be expected that the precipitation of secondary phases on previous δ/γ boundaries will be favored.

B. Effect of annealing on the microstructure

When the as-resolidified material was annealed at 900°C, the precipitation of secondary phases was observed within the ferrite phase. The microscopic examination indicate that the investigated DSS solidified at moderately high cooling rate is very prone to γ_2 and σ-phase formation.

Figures 2(a) through (f) show light optical micrographs at various stages of the decomposition of ferrite. From these figures, it is obvious that the precipitation proceeds extensively, causing large changes in the structural parameters. The observed high rate of ferrite transformation and a significant difference in extent and kinetics of precipitation between two phases are unambiguously confirmed by the results of stereological analysis. As it can be seen from the data presented in Table 1, the total volume fraction of precipitated secondary phases increases rapidly with reaction time and reaches a maximum of about 30 vol.% after 120 min of annealing. The initial transformation of δ ferrite occurs, as expected sequentially at the previous δ/γ boundaries by discontinuous (cellular) precipitation of γ_2, γ_{2b}. Annealing for 2 minutes has a little effect and the microstructure is practically unaltered. Figure 2(a) reveals the presence of γ_{2b} only on a limited number of δ/γ boundaries. However, the volume fraction of cellular γ_{2b} increased with increasing annealing time and the γ zones, already present in the as-resolidified structure ($\gamma_E + \gamma_T$) become broader. The morphological features of the cellular precipitates are illustrated by the LO and SEM micrographs of Figs.2 and 3. When GTA resolidified melt was annealed for a time period longer than 5 minutes, extremely fine γ_{2i} precipitates started to appear inside the ferrite matrix. The precipitation rate of these newly formed particles was fairly rapid. After 30 minutes of annealing the volume fraction of intragranular γ_{2i} becomes nearly equal to that of γ_{2b}. The participation of γ_{2i} and γ_{2b} in the total relative increase of the volume fraction of the γ phase:

$$\%\Delta V_{V\gamma} = (V_{V\gamma\ \text{annealed}} / V_{V\gamma\ \text{initial}} - 1)\ 100 \qquad (1)$$

is presented in Fig.4(a). These graphs show that about 90% of the $\delta \rightarrow \gamma$ transformation occurs in the first 15 – 30 minutes and then a steady state is established. Although the amount of intragranular γ_2 is low, about 3.70 vol.%, a high density of finely dispersed γ_{2i} caused an increase in the values of $S_{V\delta-\gamma}$ and $S_{V\delta-\gamma}/V_{V\gamma}$ by factor 1.42 and 1.24, respectively. In some cases, the density of γ_{2i} was so high that a so-called basket weave structure was formed,

Fig.3(b). Since in a series of recent studies (Radenković et al., 1994; Radenković et al., 1995; Cvijović et al., 1997) we have demonstrated that the pit initiation is associated with the δ/γ interphase, it should be expected that the higher amount of δ/γ boundaries arranged on shorter distances provides more sites for nucleation of pits. With further increase of annealing time coarsening of the structure by coalescence and rounding of the boundaries decreases the effect of the change of the phase composition.

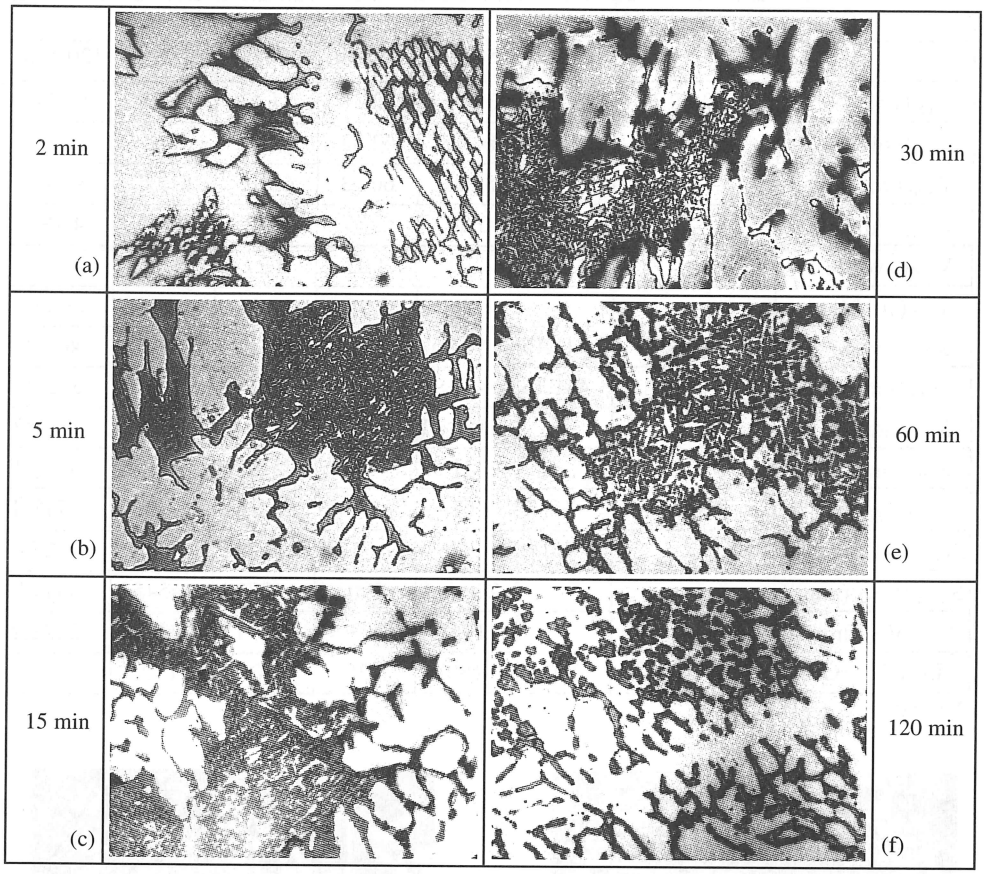

Fig.2. Microstructure of surface melted DSS after various times of annealing at 900°C.

During the early stage of annealing, the rate of σ-phase formation was also retarded, but after an incubation period of 5 minutes a great continuous increase was observed, Fig.4(b). Thus, after 30 and 60 minutes the amount of δ transformed to σ-phase was 60.5 and 68.9 %, respectively. The precipitation of σ-phase begins in the ferrite lamelle, which are chromium and molybdenum rich, Fig.2(c). In the blocky ferrite the σ particles were very dispersed and rarely identified. Other nucleation sites for σ-phase, although not frequently observed, are the new migrating δ/γ_{2b} boundaries, Fig.2(d). At later stages, when the precipitation of σ-phase was more intensive, Figs.2(e) and (f), the majority of σ particles were found to nucleate within

the ferrite matrix. The increase in fineness of its particles could have been due to accelerated nucleation. As a result, the highest value of $S_{V\sigma}$ exhibited at the end of exposure period is greater by a factor 1.73 than after 30 minutes. However, it should be pointed out that the values of $S_{V\sigma}/V_{V\sigma}$ are very similar, due to the high amount of σ-phase.

Table 1. Results of stereological analysis and electrochemical tests.

	As-resolidified	900°C					
		2 min	5 min	15 min	30 min	60 min	120 min
$V_{V\delta}$ (vol.%)	43.40	42.05	39.26	32.31	23.43	16.39	13.44
$V_{V\gamma}$ (vol.%)	56.60	57.95	60.15	62.83	64.48	64.99	65.21
$V_{V\gamma b}$ (vol.%)*		57.95	59.31	60.63	60.76	61.05	61.03
$V_{V\gamma 2i}$ (vol.%)		-	0.84	2.20	3.72	3.94	4.18
$V_{V\gamma 2b}$ (vol.%)		1.35	2.71	4.03	4.27	4.45	4.43
$V_{V\sigma}$ (vol.%)		-	0.59	3.76	12.09	18.62	21.35
$S_{V\gamma}$ (mm^{-1})	462.00	441.16	613.08	628.04	653.86	603.20	465.23
$S_{V\gamma b}$ (mm^{-1})*		441.16	430.97	432.12	427.94	424.11	322.41
$S_{V\gamma 2i}$ (mm^{-1})		-	182.11	195.92	225.92	179.09	142.82
$S_{V\sigma}$ (mm^{-1})		-	11.52	78.55	274.67	411.41	474.23
$S_{V\gamma}/V_{V\gamma}$ (mm^{-1})	816.25	761.3	1019.3	999.6	1014.1	928.1	713.4
$S_{V\gamma b}/V_{V\gamma b}$ (mm^{-1})*		761.3	726.6	712.7	704.3	694.7	527.4
$S_{V\gamma 2i}/V_{V\gamma 2i}$ (mm^{-1})		-	21679.8	8905.5	6073.1	4545.4	3416.7
$S_{V\sigma}/V_{V\sigma}$ (mm^{-1})		-	1965.9	2089.1	2271.9	2209.5	2221.2
E_P, mV (SCE)	570	530	150	125	30	120	70

* $\gamma_b = (\gamma_E + \gamma_T + \gamma_{2b})$

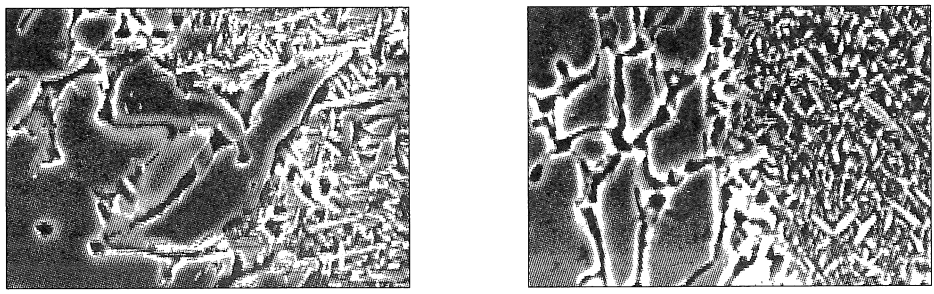

(a) 3 μm (b) 3 μm

Fig.3. SEM micrographs showing γ_{2b} formed at previous δ/γ boundaries by cellular precipitation and γ_{2i} in the form of a basket weave structure.

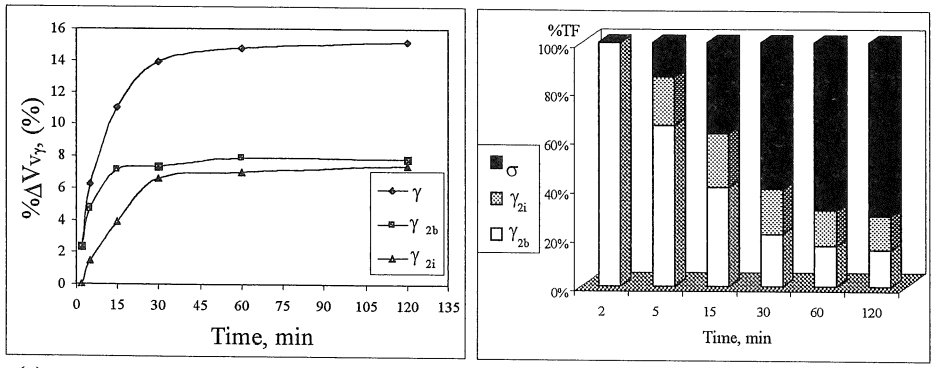

(a) (b)

Fig. 4. Effect of annealing time on the relative increase in the total volume fraction of austenite, $\%\Delta V_{V\gamma}$, and participation of γ_{2i} and γ_{2b} in $\%\Delta V_{V\gamma}$ (a), and the amount of decomposed δ which is transformed in γ_{2i}, γ_{2b} and σ (b).

C. Sensitivity to pitting corrosion

The results of electrochemical tests have shown that resolidification is quite effective in ennobling the pitting potential of investigated DSS. Namely, the E_P value corresponding to as-resolidified GTA melt is for about 400 mV more noble than the corresponding to the as-cast base material. However, in accordance with expectations the anodic polarization curves, Fig.5, and values of pitting potential, E_P, given in Table 1, clearly demonstrate that the applied heat treatment results in a drastic decrease of pitting corrosion resistance.

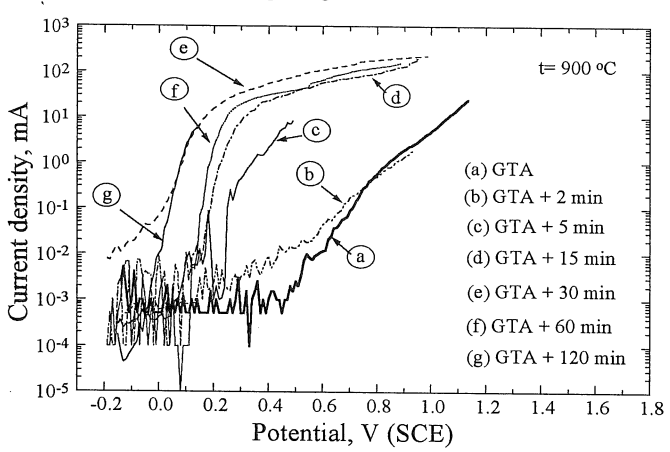

Fig.5. Anodic polarization curves.

In the early annealing stages the E_P value decreased gradually, due to the presence of a small amount of γ_2. After 5 minutes of annealing, the trend was changed. The simultaneous formation of γ_2 and σ-phase resulted in a significant decrease of the pitting corrosion resistance. Owing to the rapid the growth of precipitated and nucleation of new σ particles, a steep fall in the E_P value occurred after 30 minutes of annealing. This drop in the E_P value

could be attributed to the depletion of chromium and molybdenum in surrounding ferrite. The LOM and SEM observations of the corroded surface support this view. In the annealed GTA melt, the pitting corrosion took place preferentially at the phase interface and grow into the ferrite adjacent to the precipitates, while the σ particles remained unattacked. The slight increase of the E_P value on further annealing may be due to a massive precipitation of σ-phase within the ferrite matrix and a consequent partitioning of alloying elements. The δ transformation was almost complete, which implies that the corrosion mechanism changed into a generalized attack.

CONCLUSION

The results of the investigation show that the microstructure of surface melted DSS with PRE_N = 32 is very sensitive to the short-time annealing at elevated temperatures. Annealing of the resolidified GTA melt at 900°C leads to δ-ferrite decomposition and large microstructural changes. The process kinetics depends on the attained degree of the thermodynamic equilibrium and initial structure morphology. The formation of finely dispersed particles of γ_2 and σ-phase causes heterogenization of the ferrite matrix and dramatically changes the corrosion behavior in 0.5M NaCl at room temperature. The σ-phase has the most deleterious effect on the pitting potential and nature of attack, due to an appreciable amount of precipitates and depletion of chromium and molybdenum in the regions adjacent to the σ particles.

REFERENCES

Cvijović Z, Knežević V, Mihajlović D. Characterization of corrosion pit morphology in terms of fractal geometry. Proc Int Conf "Q-Mat '97", Warsaw. 1997; 235-41.

Elmer WJ, Allen SM, Eagar TW. Microstructural development during solidification of stainless steel alloys. Metall Trans A 1989; 20A: 2117-131.

Kane RD. Super stainless steels. Resist hostile environments. Advan Mater Processes 1993; 7: 16-20.

Kokawa H, Kuwana T, Yamamoto A. Crystallographic characteristics of delta-ferrite transformation in a 304L weld metal at elevated temperatures. Weld J 1998; 68: 92-s-101-s.

Kotecki DJ. Heat treatment of duplex stainless steel weld metals. Weld J 1989; 68: 431-s –41-s.

Nilsson J-O, Karlsson L, Andersson J-O. Secondary austenite formation and its relation to pitting corrosion in duplex stainless steel weld metal. Mater Sci Technol 1995; 11: 276-83.

Nilsson J-O, Huhtala T, Jonsson P, Karlsson L, Wilson A. Structural stability of super duplex stainless weld metals and its dependence on tungsten and copper. Met Mater Trans A 1996; 27A: 2196-208.

Ogava T, Koseki T. Effect of composition profiles on metallurgy and corrosion behavior of duplex stainless steel weld metals. Weld J 1995; 69: 181-s–90-s.

Radenković G, Cvijović Z, Mihajlović D. Effect of quenching temperature on microstructure and properties of cast duplex stainless steel, Acta Stereol 1994; 13: 439-44.

Radenković G, Cvijović Z, Zečević SK, Mihajlović D. The influence of microstructure modified by rapid solidification on corrosion behavior of cast duplex stainless steel. Pract Met Sonderbd 1995; 26: 295-307.

Sedriks AJ. New stainless steels for sea water service. Corrosion 1989; 45: 510-18.

Shek CH, Shen GJ, Lai JKL, Duggan BJ. Early stages of decomposition of ferrite in duplex stainless steel. Mater Sci Technol 1994; 10: 306-11.

Wagner GH, Korkhaus JKL. Service experience with duplex stainless steels in the chemical industry. Matwiss u Werkstoffech 1995; 26: 191-98.

Walker RA. Duplex and high alloy stainless steels - corrosion resistance and weldability. Mater Sci Technol 1988; 4: 78-85.

Yoshioka H, Yochida S, Kawashima A, Asami K, Hashimoto K. The pitting corrosion behavior of rapidly solidified aluminium alloys. Corros Sci 1986; 26: 795-812.

Presented at the 7th European Congress for Stereology, Amsterdam, April 20th to 23rd, 1998.